View metadata, citation and similar papers at core.ac.uk

brought to you by CORE

provided by NASA Technical Reports Server

TM-72-1011-1

CASE FILE
COPY

TECHNICAL MEMORANDUM

THE BRIGHTNESS TEMPERATURE OF THE AIR-SEA INTERFACE AT MICROWAVE FREQUENCIES

Bellcomm

BELLCOMM, INC.
955 L'ENFANT PLAZA NORTH, S.W., WASHINGTON, D.C. 20024

COVER SHEET FOR TECHNICAL MEMORANDUM

TITLE- The Brightness Temperature of the Air-Sea Interface at Microwave Frequencies

TM-72-1011-1

DATE- January 21, 1972

FILING CASE NO(S)- 105-9

AUTHOR(S)-C.C.H. Tang

FILING SUBJECT(S) (ASSIGNED BY AUTHOR(S))- Brightness Temperature
Emissivity

ABSTRACT

Available results of observation have shown that at nadir the brightness temperature of the sea surface at 19.35 GHz increases linearly with increasing wind speed. The computational results of the modified theoretical model presented herein are in good agreement with the measurement results both at nadir and other angles. The model depicts that, for a fully developed sea driven by the wind with speed above 5 m/sec, the air in the transitional zone immediately above the air-sea interface is mixed with sea water droplets from bursting air bubbles. The droplet concentration has a profile tapering off to zero at a certain height. The dielectric constant of the inhomogeneous droplet profile is thus both a function of the height above the interface and the wind speed. Both the inhomogeneity effect and the possible attenuation effect of the droplet concentration have been considered.

BA-145A (8-68)

DISTRIBUTION

COMPLETE MEMORANDUM TO

CORRESPONDENCE FILES:

OFFICIAL FILE COPY
plus one white copy for each additional case referenced

TECHNICAL LIBRARY (4)

NASA Headquarters

W. O. Armstrong/MTL
P. E. Culbertson/MT
C. J. Donlan/MD-T
M. Dubin/SG
T. L. Fischetti/MLA
L. B. C. Fong/SRA
H. Hall/MT-2
R. L. Lohman/MF
D. R. Lord/MF
J. G. Lundholm/MLA
A. S. Lyman/MAP
M. W. Molloy/SRR
A. B. Park/SRR
M. J. Swetnick/SRR
M. Tepper/SRD
P. G. Thome/SRE
J. W. Wild/MTE

Goddard Space Flight Center

S. C. Freden/650
P. Gloersen/650
W. A. Hovis/652
W. Nordberg/650
R. Wexler/650

Manned Spacecraft Center

T. L. Barnett/TF4
J. E. Dornbach/TF
D. E. Evans/TF
M. R. Holter/TF
C. L. Korb/TF
A. Potter/TF

Marshall Space Flight Center

E. Stuhlinger/AD-S

Mississippi Test Facility

R. O. Piland

Air Force Cambridge Research Laboratory

K. R. Hardy
H. Ottersten
C. Sletton

Johns Hopkins University

I. Katz

Massachusetts Institute of Technology

D. H. Staelin

Stanford Research Institute

D. Parker
L. Young

University of Michigan

D. C. Anding
F. C. Polcyn

Aerojet-General Corporation

H. G. Pascalar
A. Stogryn

General Electric Company

K. Tomiyasu

U.S. Naval Research Laboratory

N. W. Guinard
J. P. Hollinger

BA-146 (8-64)

DISTRIBUTION LIST (Cont'd.)

Bellcomm

A. P. Boysen, Jr.
F. El-Baz
J. O. Cappellari, Jr.
K. R. Carpenter
N. W. Hinners
M. Liwshitz
H. S. London
J. M. Nervik
G. T. Orrok
W. Strack
M. P. Wilson
All Members Department 1011
Department 1022 & 1025 Supervision
Department 1024 Files

Abstract Only to

Bellcomm

J. P. Downs
I. M. Ross
R. L. Wagner

Bellcomm

955 L'Enfant Plaza North, S.W.
Washington, D. C. 20024

date: January 21, 1972

to: Distribution

TM-72-1011-1

from: C.C.H. Tang

subject: The Brightness Temperature of the Air-Sea Interface at Microwave Frequencies - Case 105-9

TECHNICAL MEMORANDUM

I. Introductory Review

In the last few years considerable efforts have been made both theoretically and experimentally in studying the characteristics of microwave emission from a wind-driven sea. The first extensive measurement of the brightness temperature of a sea was made in 1968 at 19.35 GHz by Nordberg et al[1] with a Convair-990 jet aircraft. Their observed results are reproduced in Figure 1 which also shows the results of the theoretical model developed by Stogryn[2] in 1967. In his model, he made use of the sea slope measurements by Cox and Munk[3] who related the density of the reflected images of the sun to the statistics of the wave slopes and found that the slope distributions were nearly Gaussian. From Figure 1 we note that over the calm sea there is general agreement between the observation and the theory if a vertical scale shift is allowed. In contrast, there is apparent disagreement between observations and Stogryn's theoretical results at 14 m/sec wind speed. The observed results for the case of 14 m/sec wind speed show at all nadir angles an almost uniform increase of temperature over those for the case of calm sea; the theoretical analysis, however, calls for a slight decrease in temperature at nadir. It has been speculated[1] that the

discrepancy at high wind speeds might be due to the effect of sea foam which has not been taken into account in Stogryn's analysis. Nordberg et al[4] made another extensive measurement of microwave emission at 19.35 GHz from the North Atlantic Ocean surface in 1969. Their observation results are reproduced in Table I and Figure 2, and they estimated from Figure 2 that the measured difference between the results of the two wind speeds is at least 22°C (after corrections for sky noise and atmospheric emission) at all nadir angles. In addition they established from the results of Table I (after corrections for sky noise and atmospheric emission) that for wind speed exceeding 5 or 6 m/sec the brightness temperature at nadir increases almost linearly with increasing wind speed at a rate of 1.2°C (meter per sec)$^{-1}$. Although these two groups of observations certainly contain some measurement inaccuracy, it appears that these measurements clearly establish the fact that at nadir the brightness temperature increases with increasing wind speed. On the other hand the theoretical analysis of Stogryn predicts the contrary.

In view of the discrepancy between the theoretical model and the observation, a brief comparison of available theoretical models and their corresponding results is in order. A search of Russian literature reveals that Shifrin and Ionina[5] made a theoretical analysis on the same subject using also the sea slope measurements by Cox and Munk[3] as Stogryn[2] did. Both models do not consider the effects of foam formation. Shifrin explicitly expressed the angle between the incident beam and the local normal $\hat{n}$ to the sea area selected for observation in terms of the angle between the direction of observation and the normal $\hat{z}$ to the horizon. Shifrin assumed that all wind directions are equally probable whereas Stogryn assumed that the crosswind case is different from the upwind case. They also used differential scattering coefficients in different forms. Because of these differences in theoretical

modeling, their results also appear somewhat different as shown in Figure 3* and Figure 4 for three typical wind speeds. We note that for the horizontal (or vertical) polarization at large nadir angles the emissivity of Stogryn's model rises (or drops) much faster at high wind speed than that of Shifrin's. For the vertical polarization at nadir, the two models show opposite predictions. On the other hand both models predict that at nadir the emissivity for the horizontal polarization decreases with increasing wind speed, in contrary to observed results. In the following section, we shall present a modified theoretical approach that models more closely the actual physical environment in the transitional zone above the air-sea interface than the presently available theoretical models do.

II. Modified Theoretical Model

The brightness temperature T_B measured by an aircraft or spacecraft at height H can be expressed as

$$T_B = \left[ET + [1-E]T_s\right]\tau(H) + \int_o^H T_A(h)\,\frac{\partial\tau(h)}{\partial h}\,dh \qquad (1)$$

where E is the emissivity of the sea surface,
T is the surface temperature of the sea,
T_s is the sky brightness temperature at the sea surface,
T_A is the temperature of the atmosphere,
and τ is the transmissivity of the atmosphere and can be expressed as

$$\tau = e^{-\sec\theta_1 \int_o^H k\rho dh},$$

---

* The author wants to thank A. Stogryn for supplying these computed data.

where ρ is the density of absorbing gases in the atmosphere,
k is the absorption coefficient for these gases,
and θ_1 is a nadir angle of observation.

Note that all the terms in Equation (1) vary sensitively according to the density profiles of absorbing gases in the atmosphere at the time of observation. These terms therefore are sources of uncertainty in theoretical computations if the water vapor profile of the atmosphere is not known during measurements. Assuming that uncertainties in these two terms could be accounted for, we shall devote the remainder of our study only on how to compute theoretically the emissivity E in a model that simulates the actual physical situation.

For a perfectly smooth air-sea interface, the emissivity can be conveniently evaluated as

$$E = 1-R \tag{3}$$

where R is the Fresnel energy reflection coefficient for either the horizontal polarization:

$$R_h = \left| \frac{\text{Cos } \theta_1 - \sqrt{\varepsilon - \text{Sin}^2\theta_1}}{\text{Cos } \theta_1 + \sqrt{\varepsilon - \text{Sin}^2\theta_1}} \right|^2 , \tag{4}$$

or the vertical polarization:

$$R_v = \left| \frac{\varepsilon \text{ Cos } \theta_1 - \sqrt{\varepsilon - \text{Sin}^2\theta_1}}{\varepsilon \text{ Cos } \theta_1 + \sqrt{\varepsilon - \text{Sin}^2\theta_1}} \right|^2 . \tag{5}$$

where ε is the complex dielectric constant of the sea water. We emphasize here that θ_1 is a nadir angle, i.e., the angle

between the direction of observation and the normal to the perfectly smooth, horizontally inclined water surface.

The wavy rough sea surface is assumed to consist of a set of smooth areas, the normals to which have a Gaussian distribution described by Cox and Munk.[3] The diffraction at the edges of an area is neglected by using the geometric optics approximation. Figure 5 shows that the true or local angle of incidence between $\hat{n}$ and the incident beam is χ. According to the definition of the Fresnel formulae, the angle χ instead of the angle θ_1 should be used in equations (4) and (5) for a wavy sea surface. We shall adopt the Shifrin approach in view of its compact computational form. Shifrin has shown that

$$E = 1 - \sec\theta_1 \int P(\theta_n(v), \phi_n(v)) \cos\chi \sec^4\theta_n R(\chi) \sin\theta_n d\theta_n d\phi_n$$

$$= 1 - 0.502 \left[\left(1+\sqrt{\frac{C}{2}}\tan\theta_1\right) R(\chi^+) + \left(1 - \sqrt{\frac{C}{2}}\tan\theta_1\right) R(\chi^-) \right]. \quad (6)$$

where $P\left(\theta_n(v), \phi_n(v)\right)$ is the Cox and Munk distribution function with coefficients that depend on the wind speed,

$$C = 0.0015 + 0.00254v, \quad (7)$$

$$\chi^+ = \cos^{-1}\left[\frac{1}{\sqrt{1+C}} \left(\cos\theta_1 + \sqrt{\frac{C}{2}}\sin\theta_1\right)\right], \quad (8)$$

and

$$\chi^- = \cos^{-1}\left[\frac{1}{\sqrt{1+C}} \left(\cos\theta_1 - \sqrt{\frac{C}{2}}\sin\theta_1\right)\right]. \quad (9)$$

Note that $\chi^+ = \chi^- = \theta_1$ when C vanishes. We also mention that (i) Eq. (6) is not to be used for v>30 m/sec, since the Cox-Munk distribution is probably no longer valid for v>30 m/sec, (ii) Eq. (6) has an error of about 1% due to integrating it by the method of steepest descents. For ε=35.62-i37.05, which is the value used by Stogryn in Fig. 3, evaluation of Eq. (6) yields the results shown in Fig. 4.

In using Eqs. (4) and (5) both Shifrin and Stogryn implied that the dielectric constant ε_o of the air immediately above the sea is unity, i.e., the effects of foam and other factors can be ignored. In physical reality, it appears that the dielectric constant ε_o of the air immediately above the sea could be a function of both the wind speed v and the height z. Eqs. (4) and (5) should take the general forms:

$$R_h = \left| \frac{\cos\chi - \sqrt{\frac{\varepsilon}{\varepsilon_o(v,z)} - \sin^2\chi}}{\cos\chi + \sqrt{\frac{\varepsilon}{\varepsilon_o(v,z)} - \sin^2\chi}} \right|^2 \tag{10}$$

$$R_v = \left| \frac{\frac{\varepsilon}{\varepsilon_o(v,z)}\cos\chi - \sqrt{\frac{\varepsilon}{\varepsilon_o(v,z)} - \sin^2\chi}}{\frac{\varepsilon}{\varepsilon_o(v,z)}\cos\chi - \sqrt{\varepsilon_o(v,z) - \sin^2\chi}} \right|^2 \tag{11}$$

We shall use Eqs. (10) and (11) in Eq. (6) as the basis to develop the modified theoretical model which we hope will simulate the actual physical environment in the vicinity of the air-sea interface as closely as possible. The essence of the problem then is to model first the dielectric constant $\varepsilon_o(v,o^+)$, i.e., immediately above the interface at $z=o^+$, as a function of the wind speed in a physically plausible manner. This will be done in the next section by utilizing all relevant information obtained from observations of the air-sea interface.

III. Dielectric Constant Model of the Air Immediately above the Air-Sea Interface

The physics of the marine atmosphere and of disturbances of the sea surface is not yet well understood. The more or less periodic disturbances of the sea surface generally originate from atmospheric, seismic, and astronomical causes and comprise a period range from about 10^{-2} to 10^5 seconds[6]. The energy is concentrated in the ordinary gravity waves (periods 1 to 30 seconds)

and in the ordinary tides (periods about 12 to 24 hours). Gravity waves are generated by the wind and mainly governed by gravitational and inertial forces. If the waves are growing or being maintained by the local wind they are called sea, whereas waves that are no longer under the action of the generating wind are termed swell. The frictional coupling between wind and sea surface is a very intricate problem. Superimposed on the big gravity waves are capillary waves (small wavelets and ripples of less than 2 centimeters in length) generally controlled by forces associated with surface tension. Evidence is growing that these tiny ripples represent the drag of the wind on the sea much more than the big waves do. Gravity waves are normally dispersive, whereas capillary waves show anomalous dispersion.

In searching for a realistic model of the transitional zone above the air-sea interface, we shall use some of the observed results that led to a partial explanation of the mechanism of sea-salt nuclei production in the atmosphere. It is known that when the wind over the sea is strong enough to create whitecaps, air is trapped by the collapsing wavecrests and rises to the sea surface in the form of small air bubbles or foam. In addition, all forms of precipitation particles are effective bubble producers when striking the sea surface as shown by Blanchard and Woodcock[7]. These air-bubbles, when bursting at the sea surface, cause a transport of sea water droplets into the air via two processes:[8] (i) the bubble film droplets and (ii) the bubble jet droplets. The droplets thus formed create a transition zone at the air-sea interface. The bubble film droplets originate from the disintegration of the bubble film, that section of the bubble that protrudes through the air-sea interface. The hemispherical film cap of a bubble rising from below breaks the surface where it is thinnest, causing a disintegration of the bubble film into hundreds of fine droplets. The bubble jet droplets emerge,

after the bursting of the film cap, from a narrow unstable jet evolving from the bottom of the collapsing bubble and then breaking into a few large droplets. Figure 6 is a reproduction from Blanchard's paper[8] showing consecutive stages of the bursting of an air bubble into jet droplets. Blanchard's experiments give the following information. The bubble diameter varies from less than a millimeter up to a centimeter and the corresponding bubble film area varied from less than $10^{-4}cm^2$ up to one cm^2. The diameter of jet droplets has a range from a few microns ($1\mu=10^{-4}$cm) up to a millimeter or so. The jet droplet ejection speed could be as high as 10^4 cm/sec and ejection height as high as 15cm. The magnitude of the jet droplet production appears to be proportional to the wind speed in the range from 5 m/sec (about 0.02 droplet $cm^{-2}sec^{-1}$) to 15 m/sec (about 0.1 droplet $cm^{-2}sec^{-1}$). The diameter of the bubble film droplets has a range from 5μ to about 20μ and these film droplets could reach a range up to more than one centimeter. The number of film droplets produced is proportional to the diameter of the film cap. A 2mm diameter bubble (film cap area about 0.005 cm^2) will produce a maximum of about 100 film droplets and a 6mm diameter bubble (film cap area about 0.3 cm^2) a maximum of 1000 film droplets. Blanchard[8,9] also showed that the percent of ocean covered with whitecaps is approximately proportional to the square of the wind speed.

It appears from the information described in the above paragraph that for a fully developed sea (i.e., wind-driven sea in a steady state) a majority of the bubbles from patches of whitecaps will spread and distribute over the sea. The bursting of these bubbles will mix the air immediately above the interface with sufficient sea water droplets to make the dielectric constant of the mixture larger than unity. It is plausible to assume that in the transitional zone the concentration of these sea water droplets will taper off from the interface to zero at a certain height according to some kind of

profile. The effect of the inhomogeneous droplet concentration profile on the transmission of the thermal emission from the sea surface will be studied later. We shall first make the following model simulating the variation of the dielectric constant of the interface air mixed with sea water droplets, the concentration of which is a function of the wind speed and the height from the interface. Immediately above the interface, a simple linear model has the form:

$$\varepsilon_o(v, o^+) = 1+(\varepsilon-1)p \tag{12}$$

where p is the percent of sea water droplets in the air immediately above the interface. Note that $\varepsilon_o(v,o^+)$ is unity for p=o and is equal to ε for p=1. We now assume that p varies as a function of the wind speed v:

$$p = c_1 + C_2 v + C_3 v^2 \tag{13}$$

The constant term C_1 takes care of the facts that (i) measurements by Nordberg et al[4] show almost no brightness temperature change for winds from calm to about 5 m/sec. (ii) the transition from a smooth sea to a sea beginning to form scattered whitecaps seems to occur at wind speeds between 5 and 7 m/sec, and Munk[10] and Mandelbaum[11] concluded that at such wind speed the sea surface undergoes an abrupt discontinuity involving the transition from laminar to turbulent flow. The linear term $C_2 v$ is consistant with the observation that the droplet production rate appears to be proportional to the wind speed at low range (5 to 15 m/sec), and the $C_3 v^2$ term indicates that the percent of whitecap coverage is approximately proportional to the square of the wind speed.

The constant C_1 can be determined in terms of C_2 and C_3 for a particular choice of v at which the whitecaps begin to appear. This v could be any number between 5 and 7

as mentioned earlier and we arbitrary choose v=5 m/sec for convenience in computation. This number also appears to be reasonable when we consult Roll's[12] Wind force chart which is reproduced here as Table II. The table indicates that at wind speeds between 4.5 and 6.6 m/sec, the sea surface has large wavelets and begins to form breaking crests and foam and perhaps scattered whitecaps. By setting p=0 and v=5 in Eq. (13), we have

$$C_1 = 5C_2 - 25C_3, \tag{14}$$

$$\text{and} \quad \varepsilon_o(v,o^+) = 1 + (\varepsilon-1)\,[(v-5)C_2 + (v^2-25)C_3] \quad \text{for } v \geq 5$$
$$= 1 \quad \text{for } v \leq 5 \tag{15}$$

Our objective now is to determine the constants C_2 and C_3, if possible, such that $\varepsilon_o(v,o^+)$ will vary with the wind speed in a manner satisfying the observed fact that at nadir the brightness temperature for the horizontal polarization increases linearly with increasing wind speed at the rate 1.2°C $(m/sec)^{-1}$.

Since $\varepsilon_o(v,o^+)$ is a function of the sea water dielectric constant ε, we must first determine ε as accurately as possible. It is well known that the dielectric constant of the sea water is a sensitive function of the emission wavelength, salinity, and temperature. An accurate evaluation of ε that represents experimental values well was not available until recently.[13] Figure 7 shows the complex dielectric constant of sea water for an average salinity of 36 parts per thousand in the North Atlantic Sea and the temperature at 7°C, which is obtained by roughly averaging sea surface temperatures for the cases shown in Table I. At 19.35 GHz (1.55cm) ε=23.41-i33.63 from Figure 7. Using this value of ε in Eqs. (15), (10), and (6), and choosing the empirical values of $C_2=6\times10^{-4}$ and $C_3=7.5\times10^{-6}$, we find that the theoretical brightness temperatures (T_B=ET) for the horizontal polarization at nadir have the observed values shown in Table III for various wind speeds.

Table III

Brightness Temperature for Horizontal Polarization at Nadir
($C_2 = 6\times10^{-4}$, $C_3=7.5\times10^{-6}$, T=280°K, ε=23.41-i33.63)

v(m/sec)	p(%)	$\varepsilon_o(v,o^+)$	T_B(°K)	ΔT_B(°K)
5	0.00	1.00-i0.00	117.9	
				5.8
10	0.36	1.08-i0.12	123.7	
				6.0
15	0.75	1.17-i0.25	129.7	
				6.2
20	1.18	1.27-i0.40	135.9	
				6.1
25	1.65	1.37-i0.56	142.0	
				6.0
30	2.16	1.48-i0.73	148.0	

Table III shows that the brightness temperature indeed increases almost linearly with increasing wind speed at a rate of 1.20°K (meter per sec)$^{-1}$. Both the percent of droplets p and the dielectric constant $\varepsilon_o(v,o^+)$ of the air and droplets mixture immediately above the interface increase also almost linearly with increasing wind speed at a rate of about 0.002-i0.03 per meter per sec. Note that $\varepsilon_o(v,o^+)$ has an attenuation part as ε does.

IV. Brightness Temperature of the Modified Theoretical Model at Other Nadir Angles

The next crucial test of the modified theoretical model is to see how well the results of the modified model agree with those of measurements at any nadir angle. The results of computation are shown in Figure 8 for the horizontal polarization. The horizontal polarization measurement curves of Figure 2 will be compared with those of Figure 8. Since the absolute calibration level of Figure 2 was not sure, Nordberg et al[4] could only estimate the brightness temperature difference (after sky noise and atmospheric emission corrections) between the curves F and B to be at least 22°K at all nadir angles.

Inspection of Figure 8 indicates that the corresponding brightness temperature difference between the curves for v=25m/sec and v=5m/sec is about 23°K at all nadir angles. The agreement is surprisingly good.

V. Effects of Inhomogeneous droplets profile on Brightness Temperature

It was mentioned in section III that the sea water droplet concentration profile could affect the transmission of the microwave emission from the sea surface. To study this problem we have to find the transmissivity of electromagnetic waves in a lossy inhomogeneous medium at an oblique indidence. This general problem has not been solved yet, but the case of lossless inhomogenous medium at normal incidence has recently been solved[14]. We shall use the results of reference [14] to get a general idea about the nature of the problem in nadir direction. To do this we must first assume the form of the droplet concentration profile F in terms of the parameter defined below:

$$\rho_h = \int_o^h \frac{2\pi}{\lambda} \sqrt{\varepsilon_o(v,z)}\, dz \qquad (16)$$

where λ is the free-space wavelength of the microwave emission, and h is the height at which $\varepsilon_o(v,h)$ is equal to unity, i.e., above h the droplets no longer contribute to the value of dielectric constant due to their sparse distribution, if any. For a profile with droplet concentration (or sea water content) decreasing with height and having at least first derivative vanishing, we assume the profile F has the form

$$F = \left[\cos\left(\frac{\pi}{2}\,\frac{\rho}{\rho_h}\right)\right]^J, \qquad J=2,3,4,..... \qquad (17)$$

where

$$\rho = \int_o^z \frac{2\pi}{\lambda} \sqrt{\varepsilon_o(v,z)}\, dz, \qquad (18)$$

with z varying from o to h, i.e., ρ varying from 0 to ρ_h Figure 9 shows the variation of F for different values of J.

The dielectric constant $\varepsilon_o(v,z)$ of the transitional zone between $z=o^+$ and z=h can then be expressed in the general form

$$\varepsilon_o(v,z) = 1 + AF = 1 + A\,[\cos(\frac{\pi}{2}\,\frac{\rho}{\rho_h})]^J, \quad (19)$$

where

$$A = \varepsilon_o(v,o^+) - 1. \quad (20)$$

Since the results of reference [14] are for the lossless case only, we have to drop the imaginary part of $\varepsilon_o(v,o)$ shown in Table III in actual computations. The computational results of the transmissivity (for normal incidence) of inhomogeneous lossless sea water droplets profiles are shown in Figure 10 for cases with J=2 and 5 and several typical values of the parameter A. The pips in the figure indicate the transmissivities of the profiles when the ratio $(\frac{h}{\lambda})$ of the profile height h to the wavelength λ of the emission is a half-wavelength. It is evident from Figure 10 that for most cases the transmissivity is practically unity when h is larger than $(3/4)\lambda$. For cases with A less than 0.3 the transmissivity is almost unity for h larger than $(1/2)\lambda$. The height h most likely will increase somewhat with increasing wind speed. Accordingly we may speculate that even at high wind speed when $\varepsilon_o(v,z)$ is relatively high, the transmissivity is close to unity for emissions with λ of the order of a few centimeters. In section III we mentioned that a bubble film could burst into hundreds of fine droplets at a height up to one to two centimeters and a bubble jet could eject a few large droplets at a height up to ten to fifteen centimeters. It appears that the bulk of droplets concentration is within the

first few centimeters for a fully developed sea. Thus for microwave emissions of wavelengths less than a few centimeters the transmissivity could be very close to unity. At longer wavelengths the transmissivity might be degraded and the problem becomes rather complicated due to multiple reflections at the interface.

What has been said in the above paragraph is true only for lossless cases. From Table III we note that $\varepsilon_o(v,o^+)$ is quite lossy, especially at high wind speeds, although in reality it may not be as lossy as indicated in the Table. The lossy part of $\sqrt{\varepsilon_o(v, o^+)}$ varies from 0.06 (for v=10m/sec) to 0.23 (for v=25m/sec). A rough estimate of the transmission loss through a lossy profile of linear form amounts from about a few percent $\left[e^{\frac{-2\pi}{\lambda}(\frac{0.06}{2})h} \text{ for v=10m/sec case}\right]$ to about 30 percent $\left[e^{\frac{-2\pi}{\lambda}(\frac{0.23}{2})h} \text{ for v=30m/sec case}\right]$ by assuming $h=(1/2)\lambda$. The effect of such a lossy profile is to reduce the measured brightness temperatures shown in Table III and Figure 8 by amounts corresponding to losses at various wind speeds. If such transmission losses are true, actual computations for any theoretical model will have to include this loss effect of an inhomogeneous droplet profile. As mentioned earlier a theoretical solution of wave transmission in a lossy inhomogeneous medium is not available yet, an accurate estimate of transmission loss in such a medium is not possible, especially under the present circumstances that experimental data on the actual sea water droplets profile and its attenuation characteristics are totally absent as far as we know.

In view of the situation, we shall assume a lossless model, i.e., $\varepsilon_o(v,o^+)$ has no attenuation part. To remove the imaginary part of $\varepsilon_o(v,o^+)$, we shall modify Eq. (12) as

$$\varepsilon_o(v, o^+) = 1 + [\tfrac{1}{2}(\varepsilon+\varepsilon^*) - 1]p \qquad (21)$$

where ε^* is the complex conjugate of ε.

Repeating the same computation procedure, we obtain $C_2=1.13\times10^{-3}$, $C_3=1.9\times10^{-5}$, and the results shown in Table IV below:

Table IV. Brightness Temperature for Lossless Model

v(^{m}/sec)	p(%)	$\varepsilon(v,o^+)$	$T_B(^oK)$	$\Delta T_B(^oK)$
5	0.00	1.00	118.6	6.0
10	0.71	1.16	124.6	6.2
15	1.51	1.34	130.8	6.1
20	2.41	1.54	136.9	5.9
25	3.40	1.76	142.8	5.9
30	4.49	2.01	148.7	

Comparison indicates that the droplets percentage p in table IV is almost twice that in Table III and $\varepsilon_o(v,o^+)$ in Table IV increases more rapidly than the real part of $\varepsilon(v,o^+)$ in Table III. Using the values of $\varepsilon(v,o^+)$ for various wind speeds in Table IV, we compute the brightness temperature for the horizontal polarization of the model at other nadir angles and obtain virtually the identical curves shown in Figure 8. This means that the values in Figure 8 are the actual measured brightness temperatures if $\varepsilon_o(v,o^+)$ is lossless and h approaches one wavelength.

The actual validity of the modified theoretical model presented herein appears to depend on future research in carrying out difficult experiments to measure the sea water droplets concentration profile and its dielectric constant and attenuation characteristics in the transitional zone above the interface of a fully developed wind-driven sea. Studies made on the attenuation characteristics of the droplets of cloud and fog might throw some light on the sea water droplets problem.

VI. Discussion and Conclusions

Ross et al[15] analyzed the similar observational data used by Nordberg et al[4] and obtained similar conclusions.

They also concluded that the predominant mechanism producing a change in T_B is more associated with changes in wind speed rather than the height of the longer gravity waves. Hollinger[16,17] made measurements from a tower (20 meters above sea surface) on a fixed ocean platform at 1.41, 8.36, and 19.34 GHz. Because of the effects of the tower structure on the brightness temperature measurements, he could not make reliable measurements between nadir and about 20° nadir angle. The absence of measurements at nadir makes it impossible to obtain the rate of brightness temperature increase at nadir with respect to the wind speed. It is evident that more measurements similar to those made by Nordberg et al[4] are needed to establish the consistency of measurements and to verify the validity of the modified theoretical model at other frequencies and for both polarizations. It is also necessary to carry out experiments to determine the sea water droplet profile and its dielectric constant and attenuation characteristics in order to understand the fundamental nature of the transitional zone at the sea-air interface. The determination of these parameters in the transitional zone is not only required for brightness temperature measurements but also has important bearing upon the capacity of the sea surface to reflect and emit light and other radiation. In turn these studies may have significant impact to the investigation of air-sea boundary layer model in weather prediction. The meteorological phenomena occuring in the immediate neighborhood of the sea surface hold a key position among all the physical processes in the marine atmosphere that is defined as being controlled by sea surface as lower boundary.

The results of the modified theoretical model are in good agreement with the measured results if the transitional zone at the air-sea interface can be considered as a lossless inhomogeneous region in which the sea water droplet profiles have heights approaching one wavelength of the radiation to be measured.

Since the brightness temperature measurements by radiometers at 19.35 GHz have established that at nadir the brightness temperature increases almost linearly with increasing wind speed for a fully developed sea, we can infer that at nadir the scattering coefficient measurements at 19.35 GHz by scatterometers should show that the scattering coefficient decreases also almost linearly with increasing wind speed. Experimental confirmation of this linear relation from scatterometer measurements will greatly enhance our understanding about the dependence of microwave emissivity and radar scattering coefficient on sea state or wind speed.

C. C. H. Tang

1011-CCHT-pal
dly

C.C.H. Tang

Attachments
References
Figures 1-10
Tables 1 and 2

REFERENCES

[1]. Nordberg, W., J. Conaway, and P. Thaddeus, "Microwave Observations of Sea State From Aircraft," Quarterly Journal of Royal Meteorological Society, 95, pp. 408-413, April, 1969.

[2]. Stogryn, A.,"The Apparent Temperature of the Sea at Microwave Frequencies," IEEE Trans. on Antenna and Propagation, 15, pp. 278-286, March 1967.

[3]. Cox, C. and W. Munk, "Measurements of the roughness of the Sea Surface from Photographs of the Sun's Glitter," Journal of Optical Society of America, 44, pp. 838-850, November 1954.

[4]. Nordberg, W., J. Conaway, D.B. Ross, and T. Wilheit, "Measurements of Microwave Emission from a Foam-Covered Wind-Driven Sea," Journal of Atmospheric Science, 28, pp. 429-435, April 1971.

[5]. Shifrin, K.S. and S.N. Jonina, "Thermal Radiation and Reflection from a Rough Sea Surface in the Microwave Region," Translation of "Perenos Mikrovolnovogo Izlucheniay v Atmospher," Trudy Glavnaya Geogizicheskaya Observatoriya, Im. A.I. Voyeykova, Number 222. Hydrometeorological Press, Leningrad, 1968.

[6]. Munk, W.H., "Origin and Generation of Waves," Proc. 1st Conference on Coastal Engineering, Long Beach, Calif., 1950, Council on Wave Research, The Engineering Foundation, pp. 1-4.

[7]. Blanchard, D.C. and A.H. Woodcock,"Bubble Formation and Modification in the Sea and its Meteorological Significance," Tellus 9, pp. 145-158, 1957.

[8]. Blanchard, D.C., "The Electrification of the Atmosphere by Particles from Bubbles in the Sea," pp. 73-197, Progress of Oceanography, Vol. 1, Editor M. Sears, MacMillan Co., 1963.

[9]. Blanchard, D.C., "Whitecaps at Sea", Journal of Atmospheric Sciences, 27, p. 645, May 1971.

[10]. Munk, W.H., "A Critical Wind Speed for Air-Sea Boundary Processes," Journal of Marine Research, 6, pp. 203-218, 1947.

[11]. Mandelbaum, H., "Evidence for a Critical Wind Velocity for Air-Sea Boundary Process", Transaction, American Geophysical Union, 37, pp. 685-690, 1956.

[12]. Roll, H.V., Physics of the Marine Atmosphere, p.24, Academic Press, 1965.

[13]. Stogryn, A., "Equations for Calculating the Dielectric Constant of Saline Water," IEEE Trans. MTT, 19, pp.733-736, August 1971.

[14]. Tang, C.C.H., "Probing Atmospheric Water Vapor Profiles Via Multiple Scattering of Electromagnetic Waves", Bellcomm Technical Memorandum 71-1011-7, November 26, 1971.

[15]. Ross, D.B., V.J. Cordone, and J.W. Conway, Jr. "Laser and Microwave Observations of Sea-Surface Condition for Fetch-Limited 17-to 25 - /sec Winds," IEEE Trans. Geoscience Electronics, 8, pp. 326-336, October 1970.

[16]. Hollinger, J.P., "Passive Microwave Measurements of the Sea Surface", Journal of Geophysical Research, 75, pp. 5209-5213, September 1970.

[17]. Hollinger, J.P., "Passive Microwave Measurements of Sea Surface Roughness", IEEE Trans. Geoscience Electronics, 9, pp. 165-169, July 1971.

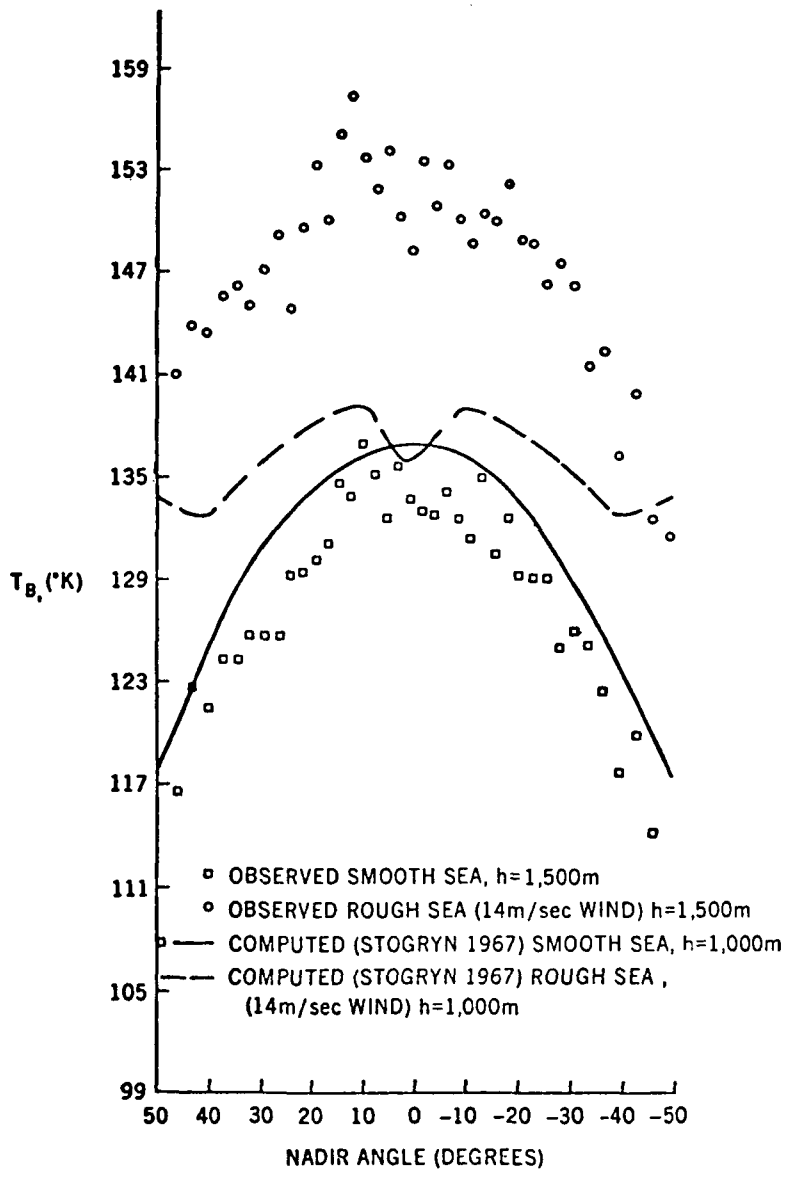

FIGURE 1 - OBSERVED AND COMPUTED (STOGRYN 1967) BRIGHTNESS TEMPERATURES VERSUS NADIR ANGLE AT 1.55 cm OVER SMOOTH AND ROUGH PORTIONS OF THE SALTON SEA. COMPUTATIONS ARE FOR SEA SURFACE TEMPERATURE OF 290°K AND A STANDARD ATMOSPHERE. OBSERVATIONS WERE MADE WITH SEA SURFACE TEMPERATURE OF 294°K OVER THE ROUGH SEA AND 300°K OVER THE SMOOTH SEA IN A RELATIVELY MOIST ATMOSPHERE ON 7 JUNE 1968. EACH POINT SHOWN FOR THE OBSERVED DATA REPRESENTS AN AVERAGE OF SIX CONSECUTIVE SCANS AT THE RESPECTIVE NADIR ANGLE

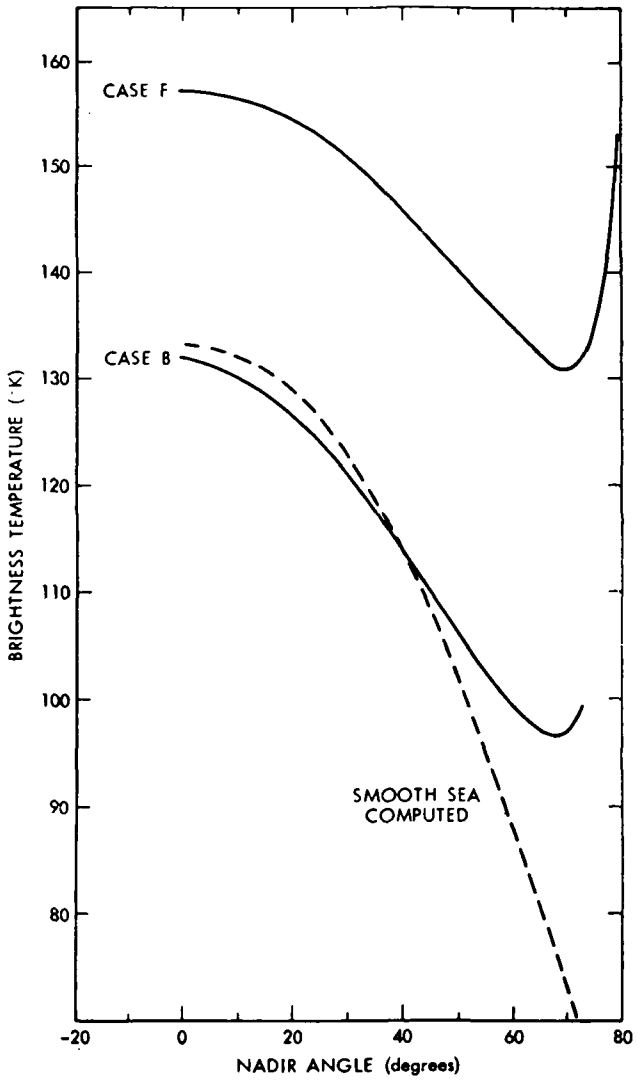

FIGURE 2 - BRIGHTNESS TEMPERATURES AVERAGED FOR 10 – 29 SEC. TIME PERIODS, FOR EACH ANTENNA SCAN ANGLE DURING 30° AIRCRAFT BANKS, VS NADIR ANGLE FOR CASE B OF TABLE 1 (LOWER CURVE) AND CASE F OF TABLE 1 (UPPER CURVE). ABSOLUTE BRIGHTNESS TEMPERATURES WERE NORMALIZED TO COMPUTATIONS FOR SMOOTH SEA (DASHED CURVE) AT NADIR. THE DASHED CURVE SHOWS COMPUTED BRIGHTNESS TEMPERATURES FOR ATMOSPHERIC AND SEA SURFACE TEMPERATURES ENCOUNTERED IN CASE B BUT FOR A SMOOTH, SPECULAR SEA SURFACE

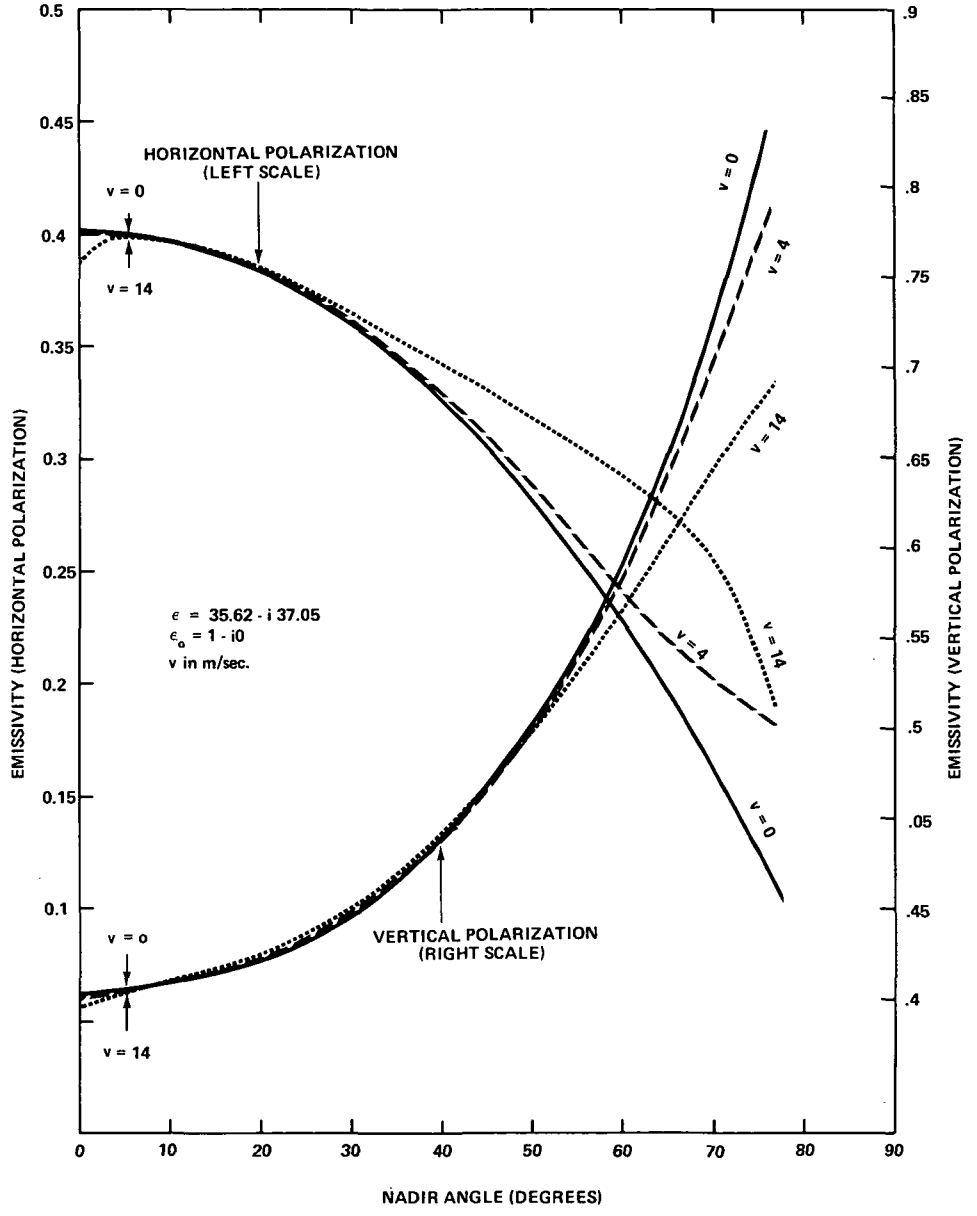

FIGURE 3 - EMISSIVITY CURVES ACCORDING TO STOGRYN

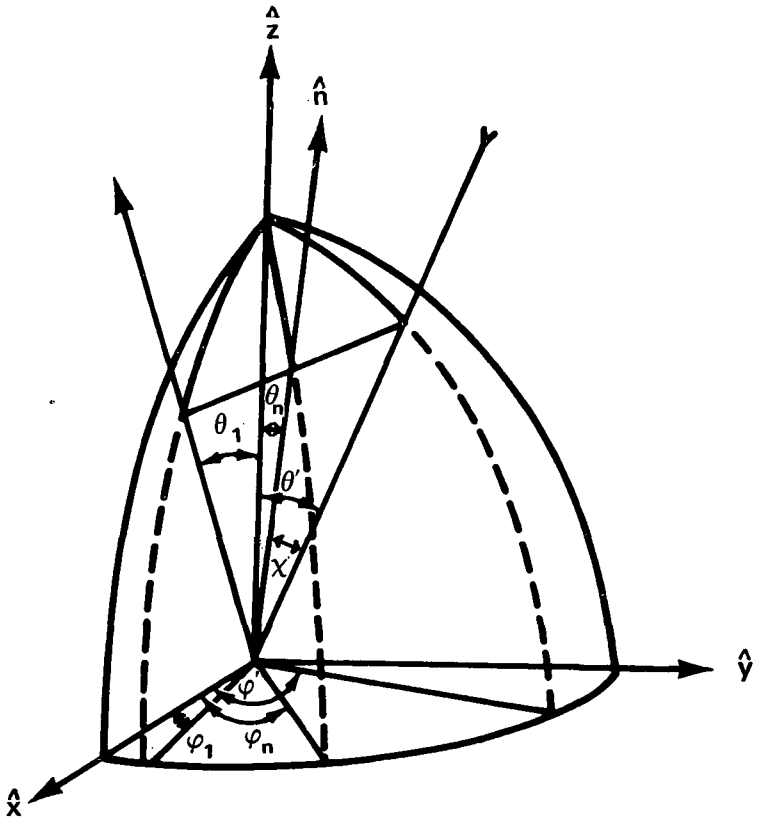

θ_1 and φ_1 are respectively the nadir angle and the azimuthal angle of the observation point.

θ' and φ' are respectively the nadir angle and the azimuthal angle of the incident beam.

θ_n and φ_n are respectively the nadir angle and the azimuthal angle of the local normal to the selected area to be observed on the surface of the sea.

χ is the true or local angle of incidence

FIGURE 5 - SCATTERING GEOMETRY

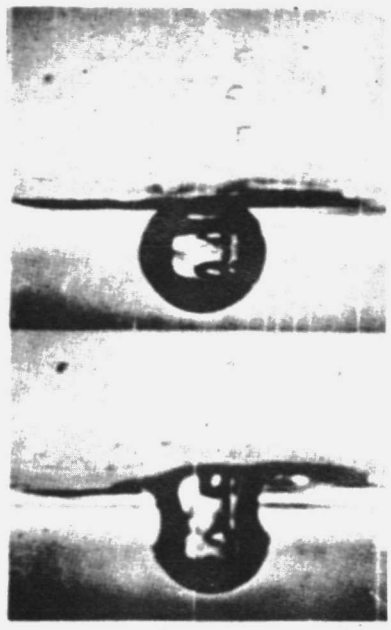

(a)

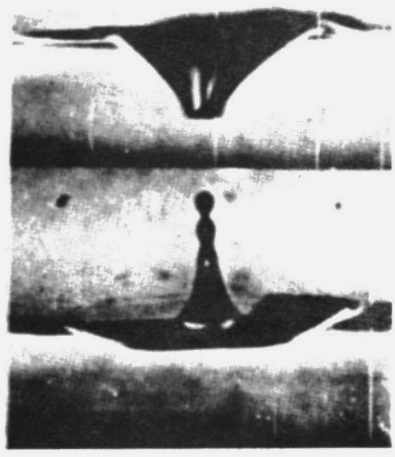

(b)

FIGURE 6 - (a) COMPOSITE VIEW OF HIGH-SPEED MOTION PICTURES ILLUSTRATING SOME OF THE STAGES IN THE COLLAPSE OF A 1.7mm DIAMETER BUBBLE. THE TIME INTERVAL BETWEEN TOP AND BOTTOM FRAMES IS ABOUT 2.3msec. THE ANGLE OF VIEW IS HORIZONTAL THROUGH A GLASS WALL. THE SURFACE IRREGULARITIES ARE DUE TO A MENISCUS. (b) OBLIQUE VIEW OF THE JET FROM A 1mm DIAMETER BUBBLE

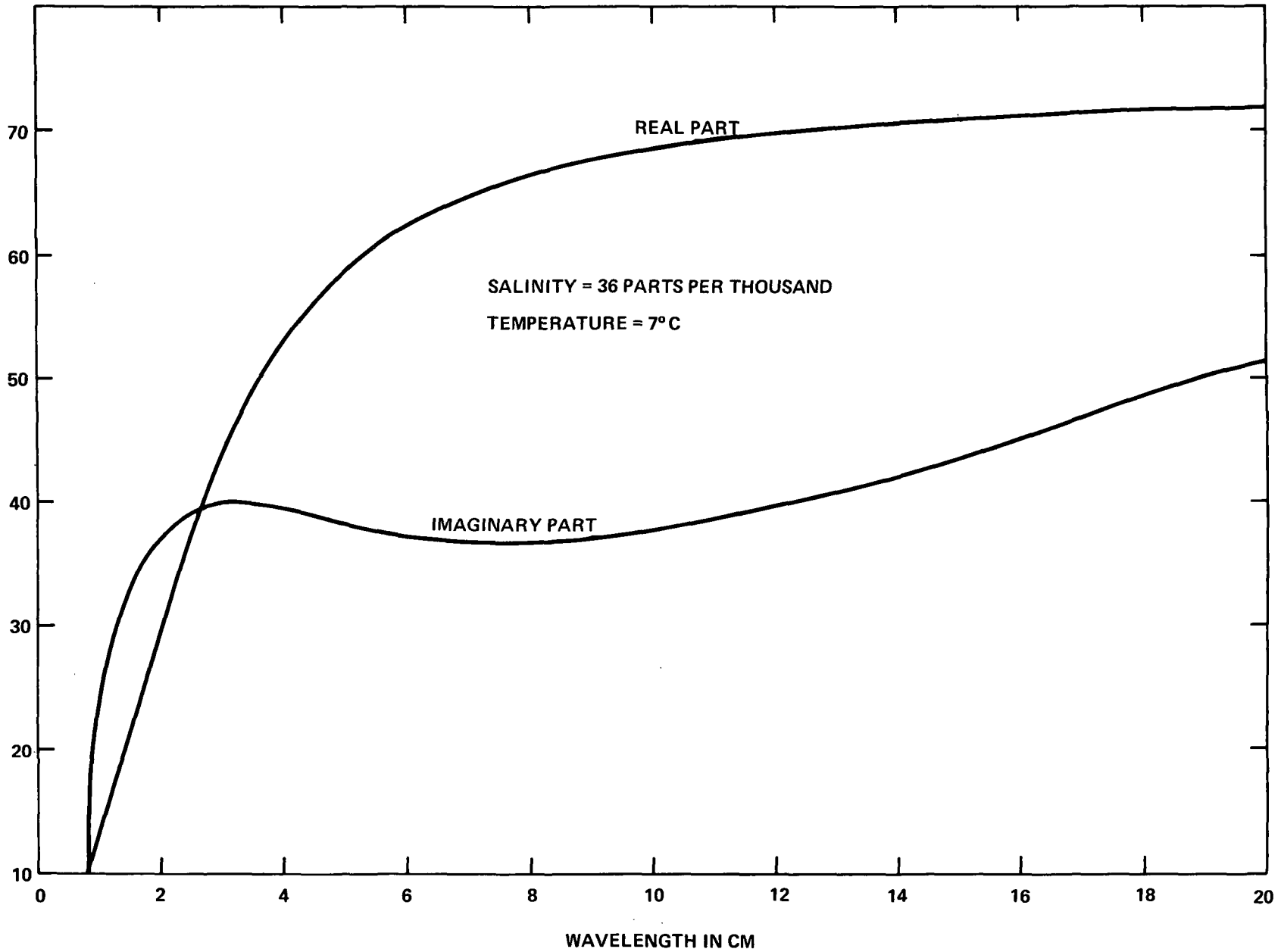

FIGURE 7 - COMPLEX DIELECTRIC CONSTANT ϵ OF SEA WATER

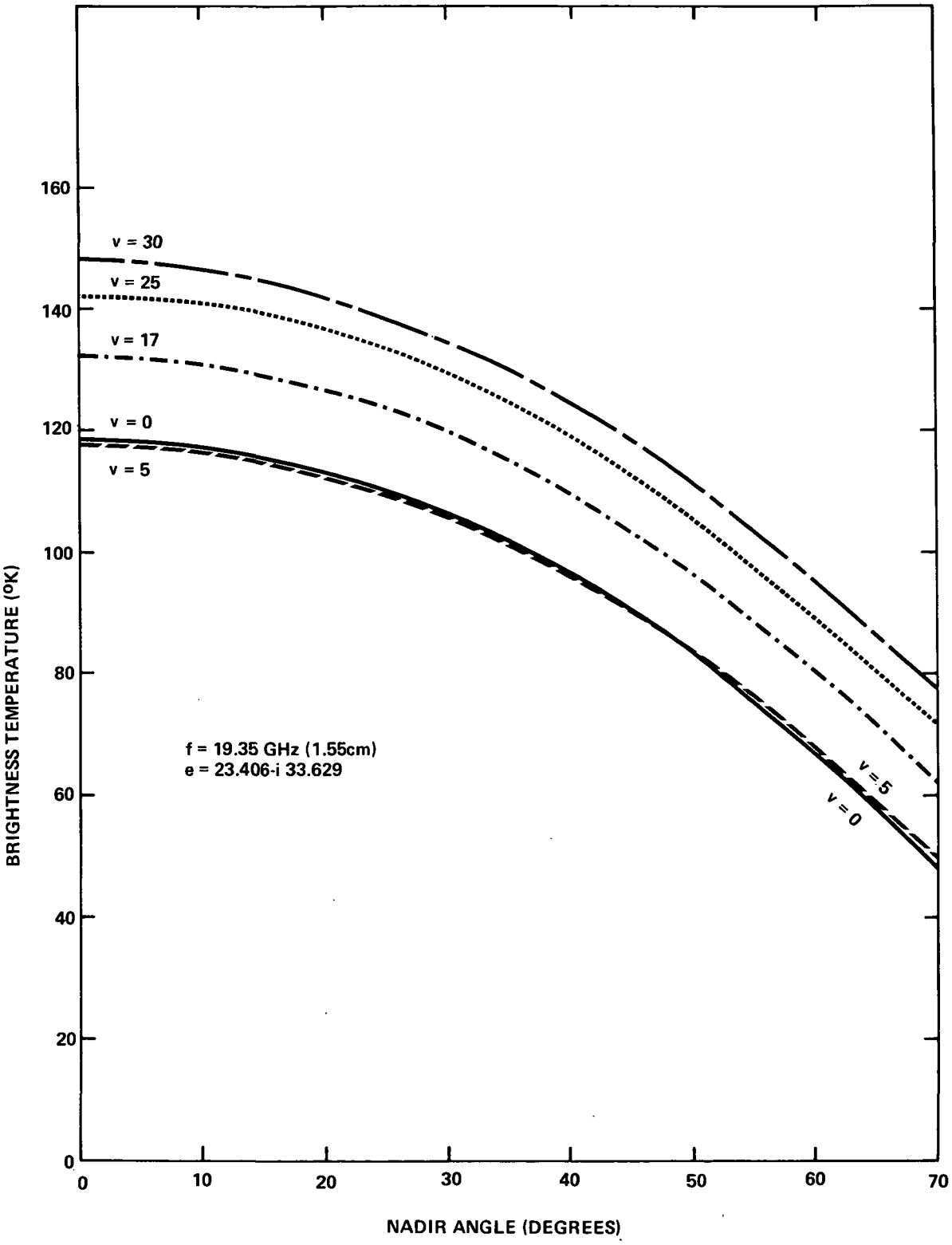

FIGURE 8 - BRIGHTNESS TEMPERATURE CURVES (MODIFIED THEORY)

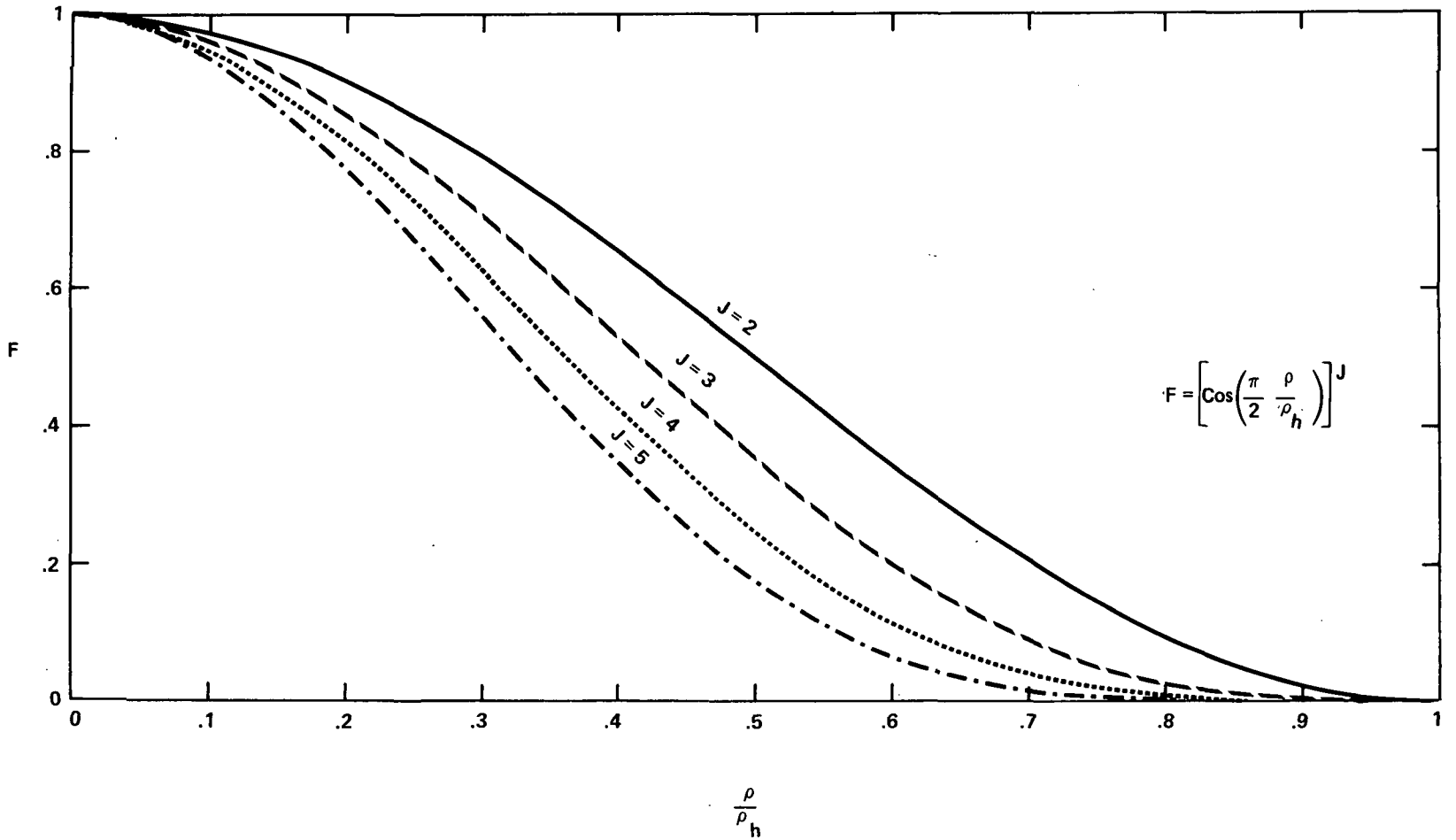

FIGURE 9 - INHOMOGENEOUS SEA WATER DROPLETS PROFILES

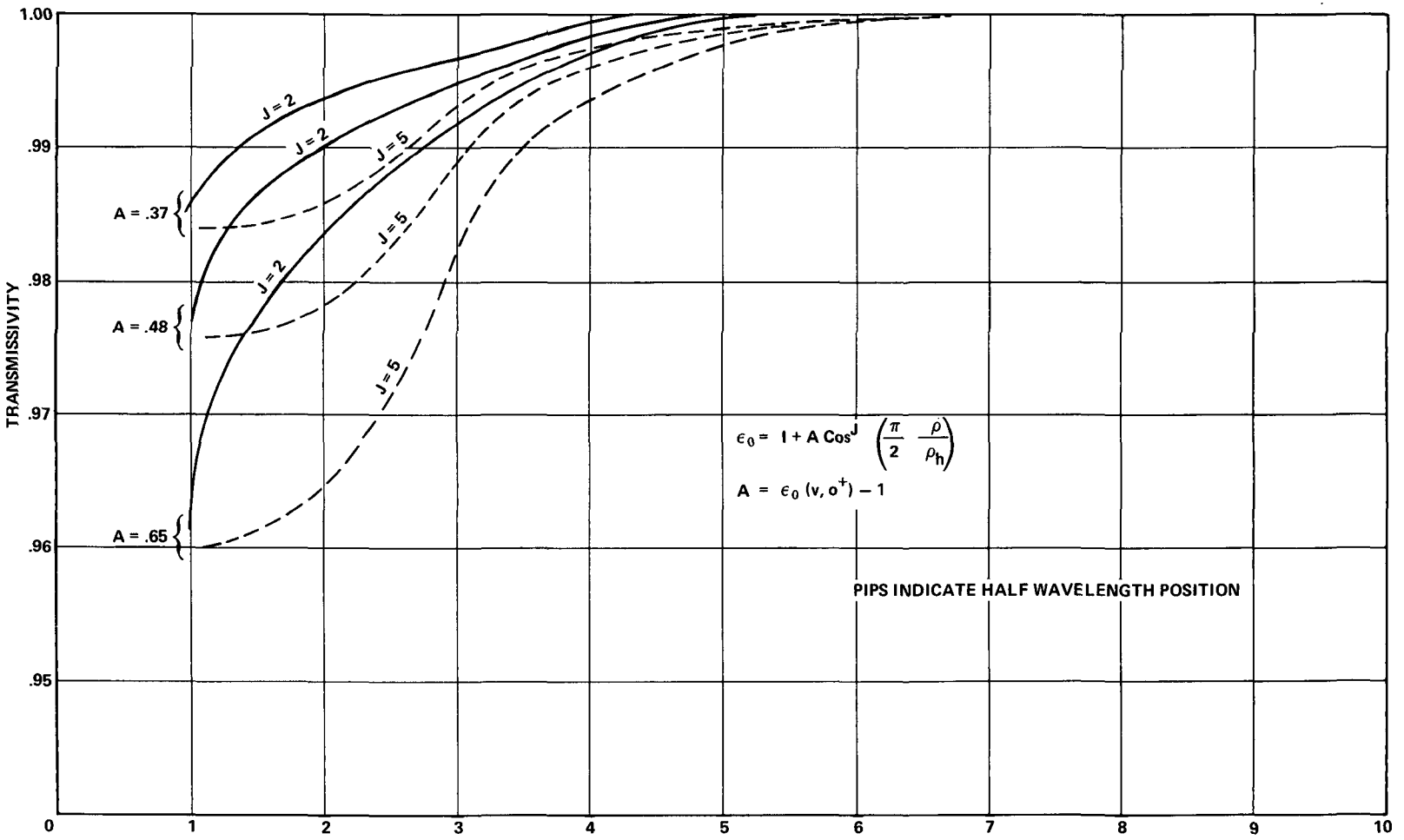

$$\rho_h = \int_0^h \frac{2\pi}{\lambda} \sqrt{\epsilon_0(v, z)}\, dz$$

FIGURE 10 - TRANSMISSIVITY (FOR NORMAL INCIDENCE) OF INHOMOGENEOUS LOSSLESS SEA WATER DROPLETS PROFILES

TABLE I

SUMMARY OF METEOROLOGICAL CONDITIONS AND MICROWAVE EMISSION TEMPERATURES FOR SIX OVERWATER FLIGHTS

	Case					
	A	B	C	D	E	F
Date (March 69)	10	13	13	10	19	14
Time (GMT)	1321	1247	1117	1430	1023	1453
Location	Atlantic Off Shannon	Atlantic Ship J	Atlantic Ship I	Atlantic Ship I	North Sea 57°N 3°E	North Sea 59°N 1°30′E
Wind speed (m sec^{-1})	<5	6	13	16	17	25
Significant wave height (m)	<1	6.0†	3.9	5.0	4.0	7.8
Foam cover (%)						
Whitecaps	—	—	4.2	5.6	6.0	5.0
Streaks	—	—	3.5	6.9	17.4	27.0
Total	—	—	7.7	12.5	23.4	32.0
Temperature (°C)						
Sea surface	9	10	9	9	2	4
Air surface	10 (est.)	11	7	5	2	2
Cloud altitude (m)						
Base	2000	clear	300	800	600	150
Top	2300	clear	2100	2000	2000	5000
Brightness temperature (°K)						
High altitude*	128**	—	—	138	138	148
Low altitude	120	118	127	132	132	142

* Measured within 30 min of time shown.
** Over Irish Sea at 1212 GMT.
† All swell, no wind waves.

TABLE II

WIND SPEED EQUIVALENTS[a] AND SPECIFICATIONS FOR THE BEAUFORT NUMBERS OF WIND FORCE

Beaufort number	Descriptive term	Wind speed equivalents				Specifications
		knots		meters/sec		
		Mean	Limits	Mean	Limits	
0	Calm	0	<1	0	<0.6	Sea like a mirror
1	Light air	3	1–4	1.5	0.7–2.3	Ripples with the appearance of scales are formed, but without foam crests
2	Light breeze	7	5–8	3.4	2.4–4.4	Small wavelets, still short but more pronounced; crests have a glassy appearance and do not break
3	Gentle breeze	11	9–12	5.6	4.5–6.6	Large wavelets; crests begin to break; foam of glassy appearance; perhaps scattered white horses
4	Moderate breeze	15	13–16	7.8	6.7–8.9	Small waves, becoming longer; fairly frequent white horses
5	Fresh breeze	19	17–21	10.2	9.0–11.3	Moderate waves, taking a more pronounced long form; many white horses are formed (chance of some spray)
6	Strong breeze	24	22–26	12.6	11.4–13.8	Large waves begin to form; the white foam crests are more extensive everywhere (probably some spray)
7	Near gale	29	27–31	15.1	13.9–16.4	Sea heaps up and white foam from breaking waves begins to be blown in streaks along the direction of the wind
8	Gale	34	32–36	17.7	16.5–19.0	Moderately high waves of greater length; edges of crests begin to break into the spindrift; the foam is blown in well-marked streaks along the direction of the wind
9	Strong gale	39	37–42	20.4	19.1–21.8	High waves; dense streaks of foam along the direction of the wind; crests of waves begin to topple, tumble, and roll over; spray may affect visibility
10	Storm	45	43–48	23.3	21.9–24.8	Very high waves with long overhanging crests; the resulting foam, in great patches, is blown in dense white streaks along the direction of the wind; on the whole, the surface of the sea takes a white appearance; the tumbling of the sea becomes heavy and shock-like; visibility affected
11	Violent storm	52	49–55	26.5	24.9–28.2	Exceptionally high waves (small- and medium-size ships might for a time be lost to view behind the waves); the sea is completely covered with long white patches of foam lying along the direction of the wind; everywhere the edges of the wave crests are blown into froth; visibility affected
12	Hurricane		>55		>28.2	The air is filled with foam and spray; sea completely white with driving spray; visibility very seriously affected

[a] Verploegh (1956).